J. Fluid Mech. (2012), *vol.* 695, *pp.* 288–309. © Cambridge University Press 2012
doi:10.1017/jfm.2012.19

Water waves over a variable bottom: a non-local formulation and conformal mappings

A. S. Fokas[1,2] **and A. Nachbin**[3]†

[1] Department of Applied Mathematics and Theoretical Physics, University of Cambridge, Cambridge CB3 0WA, UK

[2] Research Center of Mathematics of the Academy of Athens, Athens, 11527, Greece

[3] Instituto Nacional de Matemática Pura e Aplicada, Estrada D. Castorina, 110, Rio de Janeiro, RJ, CEP 22460-320, Brazil

(Received 8 September 2011; revised 21 December 2011; accepted 3 January 2012; first published online 24 February 2012)

In Ablowitz, Fokas & Musslimani (*J. Fluid Mech.*, vol. 562, 2006, pp. 313–343) a novel formulation was proposed for water waves in three space dimensions. In the flat-bottom case, this formulation consists of the Bernoulli equation, as well as of a non-local equation. The variable-bottom case, which now involves *two* non-local equations, was outlined but not explored in the above paper. Here, the variable-bottom formulation is addressed in more detail. First, it is shown that in the weakly nonlinear, weakly dispersive regime, the above system of three equations can be reduced to a system of two equations. Second, by combining the novel non-local formulation of the above authors with conformal mappings, it is shown that in the two-dimensional case, it is possible to obtain a system of two equations *without* any asymptotic approximations. Furthermore, for the weakly nonlinear, weakly dispersive regime, the nonlinear equations are simpler than the equations obtained without conformal mappings, since they contain lower order derivatives for the terms involving the bottom variable.

Key words: surface gravity waves, topographic effects

1. Introduction

A novel formulation of the classical problem in hydrodynamics of the propagation of surface waves generated by an incompressible fluid with a free surface was presented in the article by Ablowitz, Fokas & Musslimani (2006), which from now on will be referred to as AFM. This formulation is based on the general approach for studying boundary-value problems for a large class of partial differential equations introduced by one of the authors (Fokas 2000; Fokas & Sung 2005). A crucial role in this approach is played by certain non-local equations, called in Fokas (2000) the *global relations*. These equations couple appropriate transforms of all boundary values. By analysing the global relations, as well as the equations obtained from the global relations via certain transformations in the Fourier space, it is possible to obtain an explicit Dirichlet to Neumann map. Additional details of this connection are found in Haut & Ablowitz (2009), where a new non-local internal wave formulation is presented.

† Email address for correspondence: nachbin@impa.br

https://doi.org/10.1017/jfm.2012.19 Published online by Cambridge University Press

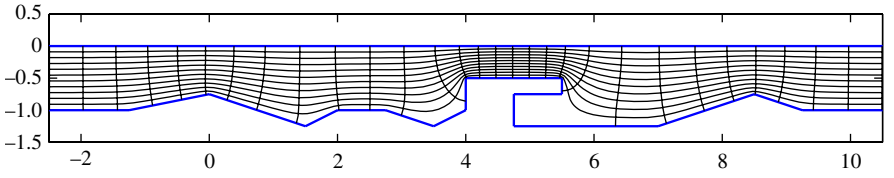


FIGURE 1. (Colour online available at journals.cambridge.org/flm) A channel with a multi-valued topography.

In the presence of a variable bottom, the formulation of AFM consists of the Bernoulli equation, as well as of two non-local equations (the two global relations). The system of these three equations characterizes the free-surface elevation $\eta(x_1, x_2, t)$, the velocity potential on the free surface $q(x_1, x_2, t)$ and the velocity potential on the variable bottom $\Phi(x_1, x_2, t)$. After presenting the above basic equations, the authors of AFM concentrated on the case of the flat bottom. The formulation of AFM has recently attracted a lot of interest, but again these works assume a flat bottom. For example, within the framework of AFM, travelling waves are analysed in Deconinck & Oliveras (2011); also, the AFM formalism is generalized in Ashton & Fokas (2011) to the case of constant vorticity, as well as to the case that the free surface is given by a multi-valued function.

Water wave problems in the case of variable bottom have been studied in a series of important papers. Peregrine (1967) made a seminal contribution, regarding a three-dimensional potential flow model with two-dimensional mild-slope bottom variations; a two-dimensional mild-slope Boussinesq system was derived, which was then followed by many other contributions found in the literature. Many of these papers investigated new strategies in order to improve the dispersive properties of the Boussinesq reduced model. Some of these references are given in the book by Mei, Stiassnie & Yue (2005). Peregrine (1967), and many others, considered small-amplitude, smooth topographies. In contrast with the mild-slope hypothesis for bottom variations, there is much less work regarding the case of large-slope, non-smooth bottom topographies. In a two-dimensional potential flow regime, Keller (2003) considered large-slope bottom variations through a boundary fitted coordinate system and presented certain constraints for a non-vanishing Jacobian. One of the authors also revisited the two-dimensional potential theory case in the presence of highly irregular bottom variations: a weakly dispersive, weakly nonlinear Boussinesq system was given in Nachbin (2003), while a fully dispersive Boussinesq-type system was presented in Artiles & Nachbin (2004), where the conformal mapping framework was combined with expansions of the Dirichlet to Neumann map; iterates of the linear Dirichlet to Neumann map were used in the equation. This weakly nonlinear, fully dispersive system was then extended to the case of nonlinear internal waves in Ruiz de Zárate *et al.* (2009). In all these cases a conformal mapping was used to generate a curvilinear coordinate system, which is also boundary fitted, but that has no restrictions regarding a vanishing Jacobian. Through the Schwarz–Christoffel mapping one can consider polygonal-shaped bottom profiles, which can be multi-valued, such as for example the roof of a submerged structure.

In this paper we concentrate on the case of the variable bottom and we include examples where the bottom variations are of large amplitude, have jump discontinuities or even present a profile which is multi-valued, such as the roof of a submerged structure (cf. figure 1). Our goal is two-fold: (a) analyse the variable-

https://doi.org/10.1017/jfm.2012.19 Published online by Cambridge University Press

bottom formulation of AFM in the weakly nonlinear, weakly dispersive regime. We find that in both the two- and three-dimensional cases, it is possible to eliminate the unknown Φ and reduce the 3×3 system to a 2×2 system for the two remaining unknown functions η and q; (b) in the two-dimensional case, we combine the approach of AFM with that of Nachbin (2003). In this way we find a 2×2 system *without* the need to make the weakly nonlinear, weakly dispersive approximation. Furthermore, if this approximation *is* assumed, we obtain a 2×2 system which appears to have certain advantages in comparison with the system obtained in (a) in the case of two dimensions. At the end of the paper an appendix is presented in two parts: (A) a straightforward description of the numerical Schwarz–Christoffel mapping of a rough channel. In a few steps this computational procedure yields discrete values for the relevant free-surface coefficients. Regarding numerical water wave dynamics, we present how to perform the mapping of surface-wave profiles between the different coordinate systems. (B) A linear dispersion analysis is presented which shows that the curvilinear coordinate setting improves computationally the *global relation* model.

2. Non-local formulation

We revisit the non-local water waves formulation of AFM. Here, we study bottom variations in more detail. Consider the three-dimensional potential theory (Euler) equations

$$\phi_{x_1x_1} + \phi_{x_2x_2} + \phi_{yy} = 0 \quad \text{with } -H'(x_1, x_2) < y < \eta(x_1, x_2, t), \tag{2.1}$$

where $\phi(x_1, x_2, y, t)$ denotes the velocity potential, $\eta(x_1, x_2, t)$ is the unknown free-surface elevation and $H'(x_1, x_2)$ denotes the known impermeable bottom (the prime emphasizes that H' is at the moment a dimensional quantity). The nonlinear boundary conditions are the kinematic condition

$$\eta_t + \phi_{x_1}\eta_{x_1} + \phi_{x_2}\eta_{x_2} - \phi_y = 0 \quad \text{on } y = \eta(x_1, x_2, t) \tag{2.2}$$

and the Bernoulli law

$$\phi_t + \tfrac{1}{2}|\nabla\phi|^2 + g\eta = 0 \quad \text{on } y = \eta(x_1, x_2, t). \tag{2.3}$$

At the bottom we have

$$\frac{\mathrm{d}\phi}{\mathrm{d}n} = 0 \quad \text{along } y = -H'(x_1, x_2). \tag{2.4}$$

The initial conditions at the free surface are

$$\phi(x_1, x_2, \eta_0, 0) = \phi_0(x_1, x_2) \quad \text{and} \quad \eta(x, 0) = \eta_0(x_1, x_2). \tag{2.5}$$

Implementing the approach introduced by one of the authors for the analysis of boundary-value problems, a novel formulation of the above problem including bottom variations was given in AFM, see (1.8), (2.3) and (2.4). However, from § 3 onwards the authors of AFM concentrated on the case of a flat bottom; thus, the dimensionless formulation presented in § 4 of AFM does not include a variable bottom.

We first revisit briefly § 4 of AFM in order to incorporate bottom variations. Recall that in AFM the original variables were denoted by primes and then the following substitutions were introduced:

$$x_1' = lx_1, \quad x_2' = \frac{l}{\gamma}x_2, \quad k_1' = \frac{k_1}{l}, \quad k_2' = \gamma\frac{k_2}{l}, \quad t' = \frac{lt}{c_0}, \quad q' = \frac{gla}{c_0}q, \quad \eta' = a\eta, \tag{2.6}$$

https://doi.org/10.1017/jfm.2012.19 Published online by Cambridge University Press

where $c_0 = \sqrt{gh_0}$ and $l, l/\gamma$ are typical length scales in the x_1 and x_2 directions. We supplement the above with

$$y' = h_0 y, \quad H' = h_0(1+H), \quad \Phi' = \frac{ac_0}{\mu}\Phi, \tag{2.7}$$

where $|H| < 1$. We recall that q' and Φ' denote ϕ' at $y' = \eta'$ and $y' = -H'$, respectively; thus, the above scaling of Φ' is consistent with the fact that

$$\frac{gla/c_0}{ac_0/\mu} = \mu\frac{gl}{c_0^2} = \mu\frac{l}{h_0} = 1; \tag{2.8}$$

the dimensionless parameters μ and ϵ are defined in AFM by

$$\mu = \frac{h_0}{l}, \quad \epsilon = \frac{a}{h_0}. \tag{2.9}$$

Using the above scalings in (1.8), (2.3) and (2.4) of AFM, dropping the effect of surface tension and introducing the notation

$$\tilde{\underline{k}} = (k_1, \gamma k_2), \quad k = |\tilde{\underline{k}}|, \quad \tilde{\nabla} \equiv (\partial_{x_1}, \gamma\partial_{x_2}), \tag{2.10}$$

we find the following basic equations:

$$q_t + \eta + \frac{\varepsilon}{2}|\tilde{\nabla}q|^2 - \frac{\varepsilon}{2}\mu^2\frac{[\eta_t + \varepsilon\tilde{\nabla}q\cdot\tilde{\nabla}\eta]^2}{1+(\varepsilon\mu|\tilde{\nabla}\eta|)^2} = 0, \tag{2.11}$$

$$\int_{-\infty}^{\infty}\int_{-\infty}^{\infty} \mathrm{d}x_1\,\mathrm{d}x_2 \mathrm{e}^{\mathrm{i}k_1x_1+\mathrm{i}k_2x_2}\left\{\mathrm{i}\eta_t\cosh(k\mu(1+\varepsilon\eta)) + \frac{1}{k\mu}(\tilde{\underline{k}}\cdot\tilde{\nabla}q)\sinh(k\mu(1+\varepsilon\eta))\right.$$
$$\left. + \frac{1}{k\mu}(\tilde{\underline{k}}\cdot\tilde{\nabla}\Phi)\sinh[k\mu H]\right\} = 0, \quad k_1, k_2 \in \mathbb{R}, \tag{2.12}$$

and

$$\int_{-\infty}^{\infty}\int_{-\infty}^{\infty} \mathrm{d}x_1\,\mathrm{d}x_2 \mathrm{e}^{\mathrm{i}k_1x_1+\mathrm{i}k_2x_2}\left\{\mathrm{i}\eta_t\sinh(k\mu(1+\varepsilon\eta)) + \frac{1}{k\mu}(\tilde{\underline{k}}\cdot\tilde{\nabla}q)\cosh(k\mu(1+\varepsilon\eta))\right.$$
$$\left. - \frac{1}{k\mu}(\tilde{\underline{k}}\cdot\tilde{\nabla}\Phi)\cosh[k\mu H]\right\} = 0, \quad k_1, k_2 \in \mathbb{R}, \tag{2.13}$$

where q and Φ denote the dimensionless forms of ϕ at $y = \eta$ and $y = -H$, respectively.

At this stage we have an integro-differential system of the three equations (2.11)–(2.13) to be solved for the surface elevation η, the velocity potential along the free surface q and the velocity potential Φ along the bottom. In the flat-bottom case, as shown in AFM, the horizontal bottom velocity $\tilde{\nabla}\Phi$ is eliminated from the dynamics and in this case Bernoulli's equation together with one non-local equation specify the surface elevation and the velocity potential along the free surface.

2.1. *The two-dimensional case*

In order to understand how to reduce the number of equations in the variable-bottom case, we first consider the two-dimensional problem. In this case, letting $x_1 = x$, (2.11)–(2.13) become the following system of three equations:

$$q_t + \eta + \frac{\varepsilon}{2}q_x^2 - \frac{\varepsilon}{2}\mu^2\frac{[\eta_t + \varepsilon q_x\eta_x]^2}{1+(\varepsilon\mu\eta_x)^2} = 0, \tag{2.14}$$

https://doi.org/10.1017/jfm.2012.19 Published online by Cambridge University Press

$$\int_{-\infty}^{\infty} \mathrm{d}x\, \mathrm{e}^{\mathrm{i}kx} \left\{ \mathrm{i}\eta_t \cosh[k\mu(1+\varepsilon\eta)] + \frac{q_x}{\mu} \sinh[k\mu(1+\varepsilon\eta)] + \frac{\Phi_x}{\mu} \sinh[k\mu H] \right\} = 0, \quad k \in \mathbb{R}, \tag{2.15}$$

$$\int_{-\infty}^{\infty} \mathrm{d}x\, \mathrm{e}^{\mathrm{i}kx} \left\{ \mathrm{i}\eta_t \sinh[k\mu(1+\varepsilon\eta)] + \frac{q_x}{\mu} \cosh[k\mu(1+\varepsilon\eta)] - \frac{\Phi_x}{\mu} \cosh[k\mu H] \right\} = 0, \quad k \in \mathbb{R}. \tag{2.16}$$

A weakly nonlinear ($\varepsilon \ll 1$), weakly dispersive ($\mu \ll 1$) model is obtained when the equations above are truncated up to a certain order in ε and μ. Recall from AFM that the following approximations can be used:

$$\cosh[k\mu(1+\varepsilon\eta)] \sim 1 + \frac{\mu^2}{2}k^2, \tag{2.17}$$

$$\sinh[k\mu(1+\varepsilon\eta)] \sim \mu k + \frac{\mu^3}{6}k^3 + \varepsilon\mu\eta k, \tag{2.18}$$

$$\sinh[k\mu H] \sim \mu k H, \quad \varepsilon, \mu \to 0. \tag{2.19}$$

Under these approximations, (2.14)–(2.16) become

$$q_t + \eta + \frac{\varepsilon}{2} q_x^2 = 0, \tag{2.20}$$

$$\int_{-\infty}^{\infty} \mathrm{d}x\, \mathrm{e}^{\mathrm{i}kx} \left\{ \left(1 + \frac{\mu^2}{2}k^2\right) \eta_t - \mathrm{i}q_x \left(k + \frac{\mu^2}{6}k^3 + \varepsilon\eta k\right) - \mathrm{i}(kH)\Phi_x \right\} = 0, \quad k \in \mathbb{R}, \tag{2.21}$$

$$\int_{-\infty}^{\infty} \mathrm{d}x\, \mathrm{e}^{\mathrm{i}kx} \left\{ \mathrm{i}\mu \left(k + \frac{\mu^2 k^3}{6} + \varepsilon k\eta\right) \eta_t + \left(1 + \frac{\mu^2}{2}k^2\right) \frac{q_x}{\mu} - \left(1 + \frac{\mu^2 k^2}{2} H^2\right) \frac{\Phi_x}{\mu} \right\} = 0, \quad k \in \mathbb{R}. \tag{2.22}$$

Using integration by parts, the weakly nonlinear, weakly dispersive equation (2.21) becomes

$$\int_{-\infty}^{\infty} \mathrm{d}x\, \mathrm{e}^{\mathrm{i}kx} \left\{ \left(1 - \frac{\mu^2}{2}\partial_{xx}\right) \eta_t + \left(\partial_{xx} - \frac{\mu^2}{6}\partial_{xxxx}\right) q + \varepsilon\partial_x(q_x\eta) + \partial_x(H\Phi_x) \right\} = 0, \quad k \in \mathbb{R}. \tag{2.23}$$

This integral is valid for any real value of k; thus, the following dispersive equation arises:

$$\left(1 - \frac{\mu^2}{2}\partial_{xx}\right) \eta_t + \left(\partial_{xx} - \frac{\mu^2}{6}\partial_{xxxx}\right) q + \varepsilon\partial_x(q_x\eta) + \partial_x(H\Phi_x) = 0. \tag{2.24}$$

Similarly, (2.22) yields the following dispersive equation:

$$\eta_{tx} - \frac{\mu^2}{6}\eta_{txxx} + \varepsilon\,(\eta\eta_t)_x - \frac{q_x}{\mu^2} + \frac{1}{2}q_{xxx} + \frac{\Phi_x}{\mu^2} - \frac{1}{2}\,(H^2\Phi_x)_{xx} = 0. \tag{2.25}$$

Equations (2.20), (2.24) and (2.25) provide a system of three equations for the three unknown functions η, q and Φ. Integrating (2.25) with respect to x and introducing the auxiliary variables

$$Q \equiv q_x, \quad \Psi_x \equiv \frac{1}{\mu^2}(\Phi_x - q_x), \tag{2.26}$$

https://doi.org/10.1017/jfm.2012.19 Published online by Cambridge University Press

the system above yields the following weakly nonlinear, weakly dispersive system of equations:

$$Q_t + \eta_x + \frac{\varepsilon}{2}(Q^2)_x = 0, \tag{2.27}$$

$$\eta_t + [(1+H)Q]_x + \varepsilon(\eta Q)_x - \frac{\mu^2}{2}\eta_{txx} - \frac{\mu^2}{6}Q_{xxx} + \mu^2(H\Psi_x)_x = 0, \tag{2.28}$$

$$\eta_t + \frac{1}{2}[(1-H^2)Q]_x + \Psi + \varepsilon\eta\eta_t - \frac{\mu^2}{6}\eta_{txx} - \frac{1}{2}\mu^2(H^2\Psi_x)_x = 0. \tag{2.29}$$

It is remarkable that by using the approximation

$$\Psi = -\eta_t - \tfrac{1}{2}[(1-H^2)Q]_x + O(\varepsilon, \mu^2), \quad \varepsilon, \mu \to 0, \tag{2.30}$$

which is a direct consequence of (2.29), one can eliminate the auxiliary velocity Ψ from (2.28). Thus, the 3×3 system (2.27)–(2.29) reduces to the following 2×2 system:

$$Q_t + \eta_x + \frac{\varepsilon}{2}(Q^2)_x = 0, \tag{2.31}$$

$$\eta_t + [(1+H)Q]_x + \varepsilon(\eta Q)_x - \frac{\mu^2}{2}[1 + 2H\eta_{tx}]_x - \frac{\mu^2}{6}[1 + 3H((1-H^2)Q)_{xx}]_x = 0. \tag{2.32}$$

Note that the dispersive term involves both η and Q.

The free-surface elevation η can be eliminated from the dispersive term by using the fact that

$$\eta_t = -[(1+H)Q]_x + O(\varepsilon), \quad \varepsilon \to 0. \tag{2.33}$$

To the same order of approximation, the 2×2 system (2.31) and (2.32) can be rewritten as

$$Q_t + \eta_x + \frac{\varepsilon}{2}(Q^2)_x = 0, \tag{2.34}$$

$$\eta_t + [(1+H)Q]_x + \varepsilon(\eta Q)_x - \frac{\mu^2}{6}[((1-H)Q)_{xx} - 3H((1+H^2)Q)_{xx}]_x = 0. \tag{2.35}$$

A well-established Boussinesq system for variable depth, deduced by Peregrine (1967), is given as follows:

$$\eta_t + [(h(x) + \varepsilon\eta)U]_x = 0, \tag{2.36}$$

$$U_t + \eta_x + \frac{\varepsilon}{2}(U^2)_x + \mu^2\left(\frac{h^2(x)}{6}U_{xxt} - \frac{h(x)}{2}[h(x)\ U_t]_{xx}\right) = 0, \tag{2.37}$$

where U is the depth-averaged horizontal velocity component and $h(x) = -1 - H(x)$. This system is valid under a mild-slope hypothesis for the topography.

As in appendix A of AFM, the system (2.34)–(2.35) can be rewritten in terms of the depth-averaged velocity by using the approximations

$$Q = U - (\mu^2/3)U_{xx} + O(\varepsilon), \tag{2.38}$$

$$\eta_t = -[(1+H)U]_x + O(\varepsilon), \quad \varepsilon \to 0. \tag{2.39}$$

https://doi.org/10.1017/jfm.2012.19 Published online by Cambridge University Press

Then (2.34) and (2.35) become

$$\eta_t + [(1+H+\varepsilon\eta)U]_x + \frac{\mu^2}{2}\left[(1+H-H^2)\ ((1+H)U)_{xx} - \left(1+\frac{2}{3}H\right)U_{xx} - H\,(H_x(1+H)U)_x\right]_x = 0, \tag{2.40}$$

$$U_t + \eta_x + \frac{\varepsilon}{2}(U^2)_x - \frac{\mu^2}{3}U_{xxt} = 0. \tag{2.41}$$

In the absence of bottom variations ($H \equiv 0$), this is the classical Boussinesq system and it coincides with the system of Peregrine. However, it is interesting to note that the topographic forcing enters in different ways in each reduced model. Peregrine's model was derived in the classical power-series fashion where both the kinematic condition and the Bernoulli law were expanded in a power series about the bottom. On the other hand, in AFM's non-local formulation, the kinematic condition is built into the Bernoulli law in an exact fashion and the kinematic condition is used without any approximation in the global relation. Hence, a 3×3, fully nonlinear, water wave system is obtained, including two non-local differential equations. In order to characterize the underlying weakly nonlinear, weakly dispersive dynamics represented by this model, these non-local equations are simplified by expanding the Fourier symbol-like terms about the free surface. This was achieved above by expanding the hyperbolic functions within the global relation. This yields a new variable-coefficient structure, when compared to known models.

The important question of how well (2.36)–(2.37) and (2.40)–(2.41) approximate the full non-local equations remains open. Another open problem is the study of the scattering properties of solitary waves characterized by these two systems. In what follows, we only look briefly at the associated dispersion relations.

The dispersion relation for both models (2.36)–(2.37) and (2.40)–(2.41) is

$$\frac{\omega(k)^2}{k^2} = \frac{1}{1+\mu^2k^2/3} = 1 - \frac{\mu^2k^2}{3} + O(\mu^4k^4). \tag{2.42}$$

The dispersion relation for the model (2.31)–(2.32) is

$$\frac{\omega(k)^2}{k^2} = \frac{1+\mu^2k^2/6}{1+\mu^2k^2/2} = 1 - \frac{\mu^2k^2}{3} + O(\mu^4k^4), \tag{2.43}$$

while for the model (2.34)–(2.35) it is

$$\frac{\omega(k)^2}{k^2} = 1 - \frac{\mu^2k^2}{3}. \tag{2.44}$$

The exact dispersion relation is

$$\frac{\omega(k)^2}{k^2} = \frac{1}{\mu k}\tanh\mu k = 1 - \frac{\mu^2k^2}{3} + \frac{2}{15}\mu^4k^4 - \cdots, \tag{2.45}$$

where Padé approximations as above only capture the quadratic term. As a particular higher order example,

$$\frac{1+a(\mu^2k^2)}{1+b(\mu^2k^2)} = 1 - \frac{\mu^2k^2}{3} + \frac{2}{15}\mu^4k^4 - \cdots \tag{2.46}$$

https://doi.org/10.1017/jfm.2012.19 Published online by Cambridge University Press

when $a = 1/15$ and $b = 2/5$ (Muñoz & Nachbin 2006). Note that the model (2.34)–(2.35) is unstable for short waves.

2.2. *The three-dimensional case*

The manipulations performed for two dimensions carry over to three dimensions in the sense that we can still reduce the 3×3 system to a 2×2 system. Indeed, using the relevant ($\varepsilon \ll 1$, $\mu \ll 1$) approximations for the hyperbolic functions in (2.12) and (2.13), we find the following equations:

$$\int_{-\infty}^{\infty}\int_{-\infty}^{\infty} \mathrm{d}x_1\,\mathrm{d}x_2 \mathrm{e}^{\mathrm{i}(k_1x_1+k_2x_2)} \left\{ \mathrm{i}\eta_t \left(1 + \frac{\mu^2}{2}k^3\right) + \frac{1}{k\mu}(\tilde{\underline{k}}\cdot\tilde{\nabla}q)\left(\mu k\left(1 + \frac{\mu^2k^2}{6} + \varepsilon\eta\right)\right) + \frac{1}{k}(\tilde{\underline{k}}\cdot\tilde{\nabla}\Phi)(kH)\right\} = 0, \quad k_1, k_2 \in \mathbb{R}, \tag{2.47}$$

$$\int_{-\infty}^{\infty}\int_{-\infty}^{\infty} \mathrm{d}x_1\,\mathrm{d}x_2 \mathrm{e}^{\mathrm{i}(k_1x_1+k_2x_2)} \left\{ \mathrm{i}\eta_t \left(\mu k\left(1 + \frac{\mu^2k^2}{6} + \varepsilon k\eta\right)\right) + \frac{1}{k\mu}(\tilde{\underline{k}}\cdot\tilde{\nabla}q)\left(1 + \frac{\mu^2k^2}{2}\right) - \frac{1}{k\mu}(\tilde{\underline{k}}\cdot\tilde{\nabla}\Phi)\left(1 + \frac{k^2\mu^2H^2}{2}\right)\right\} = 0, \quad k_1, k_2 \in \mathbb{R}. \tag{2.48}$$

Integrating by parts yields the following formal substitutions:

$$k_j \to i\partial x_j, \quad j = 1, 2, \quad \text{and} \quad k^2 \to -\tilde{\Delta} \equiv \tilde{\nabla}\cdot\tilde{\nabla}. \tag{2.49}$$

Neglecting terms of order $O(\varepsilon, \mu^2)$, (2.47) yields

$$\eta_t - \frac{\mu^2}{2}\tilde{\Delta}\eta_t + \tilde{\Delta}q - \frac{\mu^2}{6}\tilde{\Delta}^2q + \varepsilon(\tilde{\nabla}\cdot\eta\tilde{\nabla}q) + \mu(\tilde{\nabla}\cdot H\tilde{\nabla}\Phi) = 0. \tag{2.50}$$

This is the same as (5.1) in AFM except that a bottom forcing term has been introduced through the last term. As in the two-dimensional case, it is convenient to introduce an auxiliary velocity function Ψ_{x_j}, such that

$$\Psi_{x_j} \equiv \frac{1}{\mu^2}\left(\Phi_{x_j} - q_{x_j}\right), \quad j = 1, 2. \tag{2.51}$$

Then (2.50) becomes

$$\eta_t - \frac{\mu^2}{2}\tilde{\Delta}\eta_t + \tilde{\Delta}q - \frac{\mu^2}{6}\tilde{\Delta}^2q + \tilde{\nabla}\cdot H\tilde{\nabla}q + \varepsilon(\tilde{\nabla}\cdot\eta\tilde{\nabla}q) + \mu^2(\tilde{\nabla}\cdot H\tilde{\nabla}\Psi) = 0. \tag{2.52}$$

Neglecting terms of order $O(\varepsilon, \mu^2)$, (2.48) yields

$$-\tilde{\Delta}\eta_t - \frac{\mu^2}{2}\tilde{\Delta}^2q - \tilde{\Delta}\Psi + \frac{\mu^2}{6}\tilde{\Delta}^2\eta_t - \varepsilon\tilde{\Delta}(\eta\eta_t) + \frac{1}{2}\tilde{\Delta}(\tilde{\nabla}\cdot H^2\tilde{\nabla}q) + \frac{\mu^2}{2}\tilde{\Delta}(\tilde{\nabla}\cdot H^2\tilde{\nabla}\Psi) = 0. \tag{2.53}$$

Integrating with respect to $\tilde{\Delta}$ leads to the approximation

$$\Psi \sim -\eta_t - \frac{\mu^2}{2}\tilde{\Delta}q + \frac{1}{2}(\tilde{\nabla}\cdot H^2\tilde{\nabla}q). \tag{2.54}$$

Substituting this approximation in (2.52), it is possible to eliminate the unknown velocity term along the bottom. Thus, we have eliminated one differential equation from our 3×3 system. The Bernoulli law remains as in (2.11).

https://doi.org/10.1017/jfm.2012.19 Published online by Cambridge University Press

In summary, we have obtained the following 2×2 Boussinesq-type system:

$$q_t + \eta + \frac{\varepsilon}{2}|\tilde{\nabla} q|^2 - \frac{\varepsilon}{2}\mu^2 \frac{[\eta_t + \varepsilon(\tilde{\nabla}\eta \cdot \tilde{\nabla} q)]^2}{1 + (\varepsilon\mu)^2 |\tilde{\nabla}\eta|^2} = 0, \tag{2.55}$$

$$\eta_t - \frac{\mu^2}{2}\tilde{\Delta}\eta_t + \tilde{\Delta} q - \frac{\mu^2}{6}\tilde{\Delta}^2 q + \tilde{\nabla} \cdot H\tilde{\nabla} q + \varepsilon(\tilde{\nabla} \cdot \eta\tilde{\nabla} q) + \mu^2(\tilde{\nabla} \cdot H\tilde{\nabla}\Psi) = 0, \tag{2.56}$$

where

$$\Psi = -\eta_t - \frac{\mu^2}{2}\tilde{\Delta} q + \frac{1}{2}(\tilde{\nabla} \cdot H^2\tilde{\nabla} q). \tag{2.57}$$

In the next section, by combining the approach of AFM with conformal mappings, we will show that it is possible to eliminate one of the non-local relations *without* using the weakly nonlinear, weakly dispersive approximations.

3. Formulation in curvilinear coordinates

When the bottom varies in a non-smooth fashion, the formulation above can be adapted to a new (more convenient) coordinate system. In this section, we show that through a change of coordinate system it is possible to again reduce the equations to a 2×2 system even in the presence of a bottom topography with corners or multi-valuedness. Moreover, this is done at the level of the non-local equations and therefore is not restricted to the weakly nonlinear, weakly dispersive regime. The optimal change of variables in two dimensions (2D) is done through a conformal mapping, and therefore it cannot be fully extended to three dimensions (3D). However, as will be shown in future publications, there exist interesting physical three-dimensional problems in which it is possible to use this approach.

3.1. *The two-dimensional case*

In the 2D case, an orthogonal curvilinear coordinate system can be obtained through the conformal mapping $z = f(w)$ of a canonical uniform strip onto the fluid domain at rest. The canonical strip is defined in the complex w-plane, $w = \xi + \mathrm{i}\zeta$, whereas the physical channel is defined in the complex z-plane, $z = x + \mathrm{i}y$. This curvilinear coordinate system, obtained through the Schwarz–Christoffel Toolbox (Driscoll & Trefethen 2002), is depicted in figure 1. The level curves for ζ are the terrain-following curves in figure 1. More details of the conformal mapping are given later in this section. In the curvilinear system (ξ, ζ), the water wave equations take the following form (Nachbin 2003):

$$\phi_{\xi\xi} + \phi_{\zeta\zeta} = 0, \quad -h_o < \zeta < N(\xi, t), \tag{3.1}$$

with the free-surface conditions

$$|\mathrm{J}|N_t + \phi_\xi N_\xi - \phi_\zeta = 0 \quad \text{on } \zeta = N(\xi, t), \tag{3.2}$$

$$\phi_t + g\eta + \frac{1}{2|\mathrm{J}|}\left(\phi_\xi^2 + \phi_\zeta^2\right) = 0 \quad \text{on } \zeta = N(\xi, t), \tag{3.3}$$

and the bottom condition is

$$\phi_\zeta = 0 \quad \text{at } \zeta = -h_o; \tag{3.4}$$

in (3.2) and (3.3), J denotes the Jacobian $|\mathrm{J}(\xi, \zeta)| = |f'(w)|^2$. It turns out that, as a consequence of having a trivial Neumann condition, it is possible to eliminate one

https://doi.org/10.1017/jfm.2012.19 Published online by Cambridge University Press

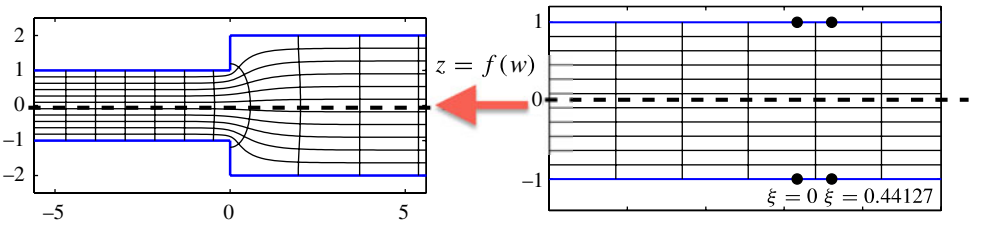


FIGURE 2. (Colour online) A channel with a step along the bottom. The dashed line represents the undisturbed free surface. A strip is mapped from the canonical w-plane onto a reflected channel in the physical z-plane.

of the two non-local equations, even in the presence of quite arbitrary topographies, provided that such topographies are allowed by the Schwarz–Christoffel transformation. These include polygonal-shaped profiles that are multi-valued.

In many cases of interest, the initial conditions are the same as before, namely

$$\phi(\xi, \eta_0, 0) = \phi_0(\xi) \quad \text{and} \quad \eta(\xi, 0) = \eta_0(\xi). \tag{3.5}$$

In other words, when a pulse-shaped wave starts propagating from a region of uniform depth, no adjustment has to be made and we simply replace x by ξ in the initial profiles. Indeed, the initial condition is not affected by the conformal mapping, since as we move into the region of constant depth the Jacobian,

$$|\mathrm{J}(\xi, \zeta)| = |\mathrm{d}z/\mathrm{d}w|^2 = y_\xi^2 + y_\zeta^2, \tag{3.6}$$

rapidly becomes equal to one. This can be illustrated through the example of figure 1, by focusing on the coordinate system in the neighbourhood of points such as $x \leqslant -2$ and $x \geqslant 10$. Clearly, we can replace x by ξ in the initial wave conditions, because at these points the transformation is nearly the identity. It is also worth noting that the Jacobian was constructed for the channel at rest and therefore it is time independent. Nevertheless, the Jacobian evaluated along the free surface is a variable coefficient in space and time. In the case of weakly nonlinear waves it can be approximated by a time-independent coefficient $M^2(\xi)$ along the free surface, namely by $y_\zeta^2(\xi, 0)$ (Nachbin 2003). These properties are important in the analysis that follows. More details of the conformal mapping are provided through the example given in figure 2.

We recall that in AFM the velocity potential along the free surface $q(x, t) = \phi(x, \eta(x, t), t)$, together with the kinematic condition, was used in order to write the free-surface dynamics only in terms of its tangential velocity $q_x(x, t)$ and $\eta(x, t)$. As mentioned in AFM, Zakharov has established that q and η are canonically conjugate coordinates, in the Hamiltonian sense. In the new formulation presented here, the same strategy can be adopted, where we now use the potential along the free surface $\zeta = N(\xi, t)$, namely

$$q(\xi, t) = \phi(\xi, N(\xi, t), t). \tag{3.7}$$

The tangential velocity is

$$q_\xi = \phi_\xi + \phi_\zeta N_\xi. \tag{3.8}$$

We write the kinematic condition in the form

$$N_t = -\phi_\xi \frac{N_\xi}{|\mathrm{J}|} + \frac{\phi_\zeta}{|\mathrm{J}|}. \tag{3.9}$$

https://doi.org/10.1017/jfm.2012.19 Published online by Cambridge University Press

Solving (3.8) and (3.9) for ϕ_ξ and ϕ_ζ, we find

$$\phi_\xi = \frac{q_\xi - |\mathrm{J}|N_\xi N_t}{1+N_\xi^2} \tag{3.10}$$

and

$$\phi_\zeta = |\mathrm{J}|N_t + N_\xi \phi_\xi = \frac{|\mathrm{J}|N_t + q_\xi N_\xi}{1+N_\xi^2}. \tag{3.11}$$

These expressions for ϕ_ξ and ϕ_ζ will be used in the Bernoulli condition in curvilinear coordinates.

The velocity potential remains harmonic in the curvilinear system. Regarding the *global relation*, following AFM we employ the harmonic function $\psi(\xi,\zeta) = \mathrm{e}^{\mathrm{i}k\xi + k\zeta}$. For two harmonic functions ϕ and ψ, the following identity holds:

$$\phi_\zeta \Delta\psi + \psi_\zeta \Delta\phi = (\phi_\zeta \psi_\xi + \psi_\zeta \phi_\xi)_\xi + (\phi_\zeta \psi_\zeta - \phi_\xi \psi_\xi)_\zeta = 0. \tag{3.12}$$

The divergence theorem, together with the fact that the normal vectors along the free surface and at the bottom are $\boldsymbol{n} = [-\eta_\xi, 1]^{\mathrm{T}}$ and $\boldsymbol{n} = [0,-1]^{\mathrm{T}}$, respectively, yields the *global relation*

$$\int_{-\infty}^{\infty} \mathrm{d}\xi \mathrm{e}^{\mathrm{i}k\xi} \left\{ \mathrm{e}^{kN}[k(\phi_\zeta - \phi_\xi N_\xi) - \mathrm{i}k(\phi_\xi + \phi_\zeta N_\xi)] + \mathrm{e}^{-kh_o}[\mathrm{i}k\Phi_\xi] \right\} = 0, \quad k \in \mathbb{R}. \tag{3.13}$$

Proceeding as in AFM, i.e. replacing in this equation the expressions for $\phi_\zeta - \phi_\xi N_\xi$, $\phi_\xi + \phi_\zeta N_\xi$ by $|\mathrm{J}|N_t$, q_ξ, and then adding to the resulting equation the equation obtained by replacing k by $-k$, we find the following equation:

$$\int_{-\infty}^{\infty} \mathrm{d}\xi \mathrm{e}^{\mathrm{i}k\xi} \left\{ \mathrm{i}|\mathrm{J}|N_t \cosh[k(h_o+N)] + q_\xi \sinh[k(h_o+N)] \right\} = 0, \quad k \in \mathbb{R}. \tag{3.14}$$

Using (3.10) and (3.11), together with the fact that $\phi_t = q_t - \phi_\zeta N_t$, the Bernoulli condition is rewritten as

$$q_t + g\eta + \frac{1}{2|\mathrm{J}|}q_\xi^2 - \frac{1}{2|\mathrm{J}|}\left[\frac{\left(|\mathrm{J}|N_t + q_\xi N_\xi\right)^2 - \left(\dfrac{1-|\mathrm{J}|^2}{1+N_\xi^2}\right) N_t^2}{1+N_\xi^2} \right] = 0. \tag{3.15}$$

Equations (3.14) and (3.15) are the two basic equations for q and N.

In the flat-bottom configuration, we have $|\mathrm{J}| \equiv 1$ ($\xi \equiv x$). Furthermore, as one moves away from regions of rough bottoms, $|\mathrm{J}|$ tends exponentially fast to 1 (Nachbin 2003). The above 2×2 system is exact, namely, even in the presence of non-smooth bottom variations, this two-dimensional nonlinear formulation contains no approximation. As described in detail in Nachbin (2003), the conformal mapping, and therefore the curvilinear coordinate system, is defined with respect to the undisturbed free-surface configuration.

Regarding weakly nonlinear expansions in ε, to be performed below, it is convenient to have y as an odd function of ζ. Therefore, the curvilinear coordinate system, generated from the conformal mapping of the canonical strip, in the w-plane, onto the physical z-plane, is established for a symmetric domain, namely the water channel reflected about its undisturbed free surface. This is depicted in figure 2, where the undisturbed free surface is indicated by a dashed line. As an illustrative example,

https://doi.org/10.1017/jfm.2012.19 Published online by Cambridge University Press

consider the case of a submerged step. This configuration has a known explicit closed formula for the conformal mapping of the lower half-domain (Floryan 1985). Namely, we consider a channel with depths $H_1 < H_2$ in the physical z-plane and a canonical strip $-h < \zeta < 0$ in the w-plane. In comparison with figure 2, Floryan's setting is vertically shifted by 1. In other words, the origin in the w-plane is mapped to the step's upper corner in such a way that $f(0) = 0$. The Jacobian is easily obtained from Floryan (1985):

$$\frac{\mathrm{d}z}{\mathrm{d}w} = \left(\frac{H_1 H_2}{h^2}\right)^{1/2} \left[\sinh\left(\frac{\pi}{2h}(w - a_1)\right)\right]^{1/2} \left[\sinh\left(\frac{\pi}{2h}(w - a_2)\right)\right]^{-1/2}, \tag{3.16}$$

where the corners' pre-images in the w-plane are given by

$$a_1 = 0, \quad a_2 = \frac{2h}{\pi}\ln(H_2/H_1). \tag{3.17}$$

This case can be integrated in closed form and yields

$$z = f(w) = \frac{H_2}{\pi}\left[\ln\frac{1+s}{1-s} - \frac{H_1}{H_2}\ln\frac{(H_2/H_1)+s}{(H_2/H_1)-s}\right] - \mathrm{i}(H_2 - H_1), \tag{3.18}$$

where

$$s^2 = \frac{\exp(w\pi/h) - (H_2/H_1)^2}{\exp(w\pi/h) - 1}. \tag{3.19}$$

Figure 2 was generated using the Schwarz–Christoffel Toolbox (Driscoll & Trefethen 2002) for the symmetric domain. The pre-images were found with great numerical accuracy as indicated in figure 2. To compute the exact value of a_2, we have used $h = 1$, $H_1 = 1$ and $H_2 = 2$. For most polygonal-shaped domains the values of the pre-images can only be found numerically, namely by solving iteratively what is known as the (nonlinear) *parameter problem* (Driscoll & Trefethen 2002). But it is worth noting that once the pre-images are found numerically, with very good accuracy, the Jacobian is readily available through the Schwarz–Christoffel mapping's expression for $\mathrm{d}z/\mathrm{d}w$ (Driscoll & Trefethen 2002).

The Jacobian in (3.14)–(3.15) is evaluated along the free surface. In other words,

$$|\mathrm{J}| = |\mathrm{J}(\xi, t)| = y_\xi^2(\xi, N(\xi, t)) + y_\zeta^2(\xi, N(\xi, t)). \tag{3.20}$$

We point out that although (3.15) is an equation in (ξ, t), it still contains the function η, which depends on (x, t). However, η can be expressed in terms of (ξ, t) using the relationship

$$x + \mathrm{i}\eta(x, t) = f(\xi + \mathrm{i}N(\xi, t)). \tag{3.21}$$

In what follows, we concentrate on the weakly nonlinear regime. For symmetric domains, it is shown in Nachbin (2003) that

$$N(\xi, t) = \frac{\eta(x(\xi, 0), t)}{M(\xi)} + O(\varepsilon^2), \quad |\mathrm{J}| = M^2(\xi) + O(\varepsilon^2),$$
$$\varepsilon \downarrow 0, \quad \text{with } M(\xi) \equiv y_\zeta(\xi, 0). \tag{3.22}$$

Before using the above approximations in (3.14) and (3.15), we first rewrite these equations in dimensionless form:

$$\int_{-\infty}^{\infty} \mathrm{d}\xi\, \mathrm{e}^{\mathrm{i}k\xi}\left\{\mathrm{i}|\mathrm{J}|N_t \cosh[k\mu(1 + \varepsilon N)] + \frac{q_\xi}{\mu}\sinh[k\mu(1 + \varepsilon N)]\right\} = 0, \quad k \in \mathbb{R}, \tag{3.23}$$

https://doi.org/10.1017/jfm.2012.19 Published online by Cambridge University Press

and

$$q_t+\eta+\frac{\varepsilon}{2|\mathrm{J}|}q_\xi^2-\frac{\varepsilon\mu^2}{2|\mathrm{J}|}\left[\frac{\left(|\mathrm{J}|N_t+\varepsilon q_\xi N_\xi\right)^2-\left(\dfrac{1-|\mathrm{J}|^2}{1+(\varepsilon\mu)^2N_\xi^2}\right)N_t^2}{1+(\varepsilon\mu)^2N_\xi^2}\right]=0. \quad (3.24)$$

As before, we use the expansions

$$\cosh[k\mu(1+\varepsilon N)]\sim 1+\frac{\mu^2}{2}k^2, \quad (3.25)$$

$$\sinh[k\mu(1+\varepsilon N)]\sim \mu k+\frac{\mu^3}{6}k^3+\varepsilon\mu Nk,\quad \varepsilon\to 0,\ \mu\to 0, \quad (3.26)$$

and integrate (3.23) by parts. Defining $Q\equiv q_\xi$, (3.23) yields

$$\left(1-\frac{\mu^2}{2}\partial_{\xi\xi}\right)(|\mathrm{J}|N_t)+\left(\partial_\xi-\frac{\mu^2}{6}\partial_{\xi\xi\xi}\right)Q+\varepsilon\partial_\xi(QN)=0. \quad (3.27)$$

Using in the above equation the approximations given in the expressions (3.22), we find

$$M\eta_t+\left[\left(1+\frac{\varepsilon\eta}{M}\right)Q\right]_\xi-\frac{\mu^2}{2}\left[(M\eta_t)_{\xi\xi}+\frac{1}{3}Q_{\xi\xi\xi}\right]=0. \quad (3.28)$$

The dispersive term can be simplified using the fact that $Q_\xi=-M\eta_t+O(\varepsilon)$. In this way we find the following weakly nonlinear, weakly dispersive Boussinesq-type system:

$$M(\xi)\eta_t+\left[\left(1+\varepsilon\frac{\eta}{M(\xi)}\right)Q\right]_\xi-\frac{\mu^2}{3}[M(\xi)\eta_t]_{\xi\xi}=0, \quad (3.29)$$

$$Q_t+\eta_\xi+\frac{\varepsilon}{2}\left[\frac{Q^2}{M^2(\xi)}\right]_\xi=0. \quad (3.30)$$

For Boussinesq-type systems, one can evaluate the velocity at different depth levels. In (3.29), Q is evaluated along the free surface. As first introduced by Nwogu (1993), we next consider an intermediate depth parameter Z_o, $0<Z_o<1$, where, for convenience, the origin has been shifted to the bottom. In this case, as shown in Nwogu (1993) (for flat bottoms) and in Muñoz & Nachbin (2006) for highly variable bottoms, one can use the approximation

$$u_o(\xi,t)\equiv\phi_\xi(\xi,Z_o,t)=\tilde{u}(\xi,t)-\frac{\mu^2}{2}Z_o^2\tilde{u}_{\xi\xi}(\xi,t)+O(\mu^4), \quad (3.31)$$

where the velocity at the bottom is denoted by $\tilde{u}\equiv\phi_\xi(\xi,0,t)$. By definition, $Q(\xi,t)=\phi_\xi+\phi_\zeta N_\xi$, which in the weakly nonlinear regime leads to

$$Q\approx\phi_\xi(\xi,1+\varepsilon N,t)=\tilde{u}(\xi,t)-\frac{\mu^2}{2}(1+\varepsilon N)^2\tilde{u}_{\xi\xi}(\xi,t)+O(\mu^4). \quad (3.32)$$

It was shown in Nwogu (1993) and Muñoz & Nachbin (2006) that taking $Z_o^2=1/3$ has the same effect as using the depth-averaged velocity, which is denoted by $U(\xi,t)$.

https://doi.org/10.1017/jfm.2012.19 Published online by Cambridge University Press

Also,

$$\tilde{u} = U + \frac{\mu^2}{6} U_{\xi\xi} + O(\mu^4), \tag{3.33}$$

which then leads to

$$Q(\xi, t) = U(\xi, t) - \frac{\mu^2}{3} U_{\xi\xi}(\xi, t) + O(\mu^4). \tag{3.34}$$

Replacing in (3.30) Q by the right-hand side of (3.34) yields the same Boussinesq-type system as the one given in Nachbin (2003):

$$M(\xi)\eta_t + \left[\left(1 + \varepsilon \frac{\eta}{M(\xi)}\right) U\right]_\xi = 0, \tag{3.35}$$

$$U_t + \eta_\xi + \frac{\varepsilon}{2}\left[\frac{U^2}{M^2(\xi)}\right]_\xi - \frac{\mu^2}{3} U_{\xi\xi t} = 0. \tag{3.36}$$

Equations (3.29)–(3.30) and (3.35)–(3.36) have the same dispersion relation as (2.42). Improved dispersion properties can be obtained by letting $Z_o = (2/3 - \sqrt{1/3})^{1/2} \approx 0.469$. This leads to a Padé approximation of the full dispersion relation with small phase errors in both the linear regime (Nwogu 1993) and the weakly nonlinear, weakly dispersive regime (Garnier, Kraenkel & Nachbin 2007) and includes the presence of rapidly varying periodic bottom topographies.

It is interesting to note that in the system (3.35)–(3.36), the Jacobian (along the undisturbed free surface) is differentiated only once. On the other hand, the systems (2.31)–(2.32), (2.34)–(2.35) and (2.36)–(2.37), which were obtained without conformal mappings, all contain second-order derivatives of the bottom profile H and hence they require more regularity of the bottom variations.

4. Conclusions

In Ablowitz *et al.* (2006), a novel formulation was proposed for water waves in three space dimensions. In this paper the variable-bottom formulation is addressed in more detail. First, it was shown that in the weakly nonlinear, weakly dispersive regime, the system of three equations can be reduced to a system of two equations. Second, by combining the novel non-local formulation with conformal mappings, it was shown that in the two-dimensional case, it is possible to obtain a system of two equations without any asymptotic approximations.

Furthermore, for the weakly nonlinear, weakly dispersive regime the nonlinear equations are simpler than the equations obtained without conformal mappings, since they contain lower order derivatives for the terms involving the bottom variable. In Muñoz & Nachbin (2005), a linear stability analysis showed that for rapidly varying topographies the eigenvalues in the Cartesian formulation were defined in a much wider interval than in the curvilinear coordinate system. This was shown to lead to improved numerical conditioning. In appendix B, we present a linear dispersion analysis of the non-local formulation which also shows changes in the conditioning behaviour (again there exists a wider frequency range in the Cartesian coordinate case, as opposed to the conformal mapping coordinates).

Regarding applications with the conformal mapping technique, appendix A contains a straightforward description of the numerical Schwarz–Christoffel mapping of a rough channel. In a few steps this computational procedure can yield discrete values for the

https://doi.org/10.1017/jfm.2012.19 Published online by Cambridge University Press

relevant free-surface coefficients. We present the numerical steps of how to perform the mapping of surface-wave profiles between the different coordinate systems.

Numerical modelling for the Boussinesq-type systems presented here is readily available by using appendix A to generate the respective variable coefficients, given a specific bottom profile, together with numerical schemes known in the literature. In particular, for solitary wave dynamics over a rough topography, a finite-difference method is available through Muñoz & Nachbin (2005, 2006). Regarding the non-local system of equations, numerical schemes have been restricted to travelling waves, in the flat-bottom case (AFM; Deconinck & Oliveras 2011). In the travelling wave case, time is eliminated from the problem, which reduces to *computational fixed point* and *computational continuation* methods. In the presence of a variable bottom, and therefore of variable coefficients, it is of interest to design and validate an efficient time-dependent scheme for the non-local equations. Xu & Guyenne (2009) recently used the Hamiltonian framework together with Dirichlet–Neumann expansions to solve numerically surface water wave problems. A symplectic implicit time integration scheme was used. Nevertheless, a de-aliasing scheme and a numerical filter were needed in order to suppress instabilities from contaminating the solution. The conclusion is that the fully time-dependent, nonlinear wave propagation through non-local formulations is a challenging numerical project. The presence of large-amplitude, non-smooth bottom variations takes the challenge to a higher degree.

Finally, the optimal change of variables in two dimensions (2D) was achieved through a conformal mapping, and therefore it cannot be fully extended to three dimensions (3D). However, as will be shown in future publications, there exist interesting physical three-dimensional problems in which it is possible to use this approach. In 3D the implementation of numerical schemes is even more challenging.

Acknowledgements

The work of A.S.F. was supported in part by the Guggenheim Foundation, USA, and by the EPSRC, UK. The work of A.N. was supported in part by CNPq under (PQ-1B) 454027/2008-7; FAPERJ project no. 112112/08 and also FAPERJ *Cientistas do Nosso Estado* project no. 102793/08.

Appendix A. Numerical Schwarz–Christoffel mapping of a rough channel

This section contains a straightforward outline for the numerical computation of the Jacobian and the free-surface coefficient $M(\xi)$. These are the variable coefficients in the non-local equations (3.14)–(3.15) and in the Boussinesq-type equations that arise and are commonly used in the modelling of long-wave disturbances in coastal regions. The presentation below shows that non-smooth, highly oscillatory topographies can be easily incorporated into standard Boussinesq models.

This section also presents the few steps needed for numerically calculating the physical wave elevation $\eta(x, t)$ from its conformally mapped counterpart $N(\xi, t)$, and *vice versa*, according to (3.21).

All the calculations described are performed using the Schwarz–Christoffel Toolbox (SCT), an open software available through Toby Driscoll's web page:
http://www.math.udel.edu/~driscoll/software/.
Once the package is downloaded an easy way to start is by running MATLAB in the directory containing all m-files. Details of the numerical schemes and issues regarding the Schwarz–Christoffel mapping are found in the book by Driscoll & Trefethen (2002).

https://doi.org/10.1017/jfm.2012.19 Published online by Cambridge University Press

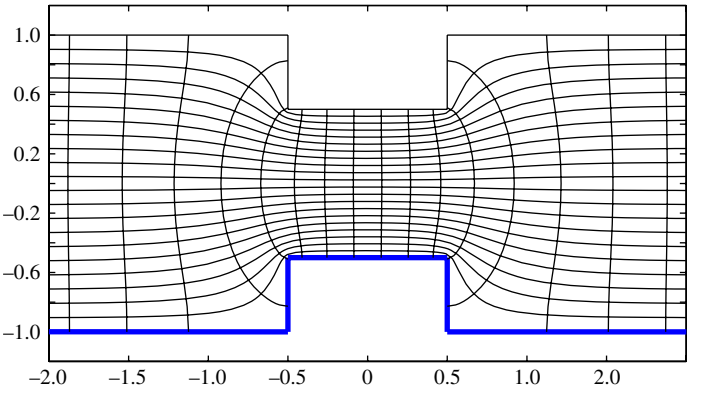


FIGURE 3. (Colour online) Symmetric channel with a submerged rectangular obstruction, depicted by the thick line. The obstruction height is equal to half the depth. The lower ($y < 0$) part of the domain represents the fluid body at rest.

A.1. *Variable coefficients connected with the topography*

Very few *commands* are necessary to compute the desired variable coefficient on a computational grid specified by the SCT user. We will describe these commands together with SCT's basic issues needed in constructing the mapping function $f(w)$. First recall that the Cauchy–Riemann equations yield the relation

$$|\mathrm{J}| = x_\zeta^2(\xi,\zeta) + y_\zeta^2(\xi,\zeta) = \left|\frac{\mathrm{d}f}{\mathrm{d}w}\right|^2. \tag{A 1}$$

As pointed out earlier, for weakly nonlinear waves $|\mathrm{J}| \approx M^2(\xi) + O(\varepsilon^2)$, where

$$M(\xi) \equiv y_\zeta(\xi,\zeta_o) = \mathrm{Re}\left\{\frac{\mathrm{d}f}{\mathrm{d}w}(\xi,\zeta_o)\right\}. \tag{A 2}$$

In the above notation: Re stands for the real part of a complex function and ζ_o denotes the undisturbed free-surface level in the canonical domain. In general, the SCT does not set the undisturbed free surface to be at $\zeta_o = 0$, which is no restriction whatsoever. The free surface variable coefficients are therefore constructed numerically by evaluating $\mathrm{d}f/\mathrm{d}w$ at mesh points, which is achieved through the command ***evaldiff***. To be more specific, let the free-surface mesh point locations be stored in the array $\boldsymbol{w}$, containing entries of the form $w_j = \xi_j + 0.5*\mathrm{i}$. As will become clear below, the undisturbed free surface is at $\zeta_o = 0.5$. From now on, the symbol >> indicates MATLAB's prompt. The command

```
>> M = real(evaldiff(f,w));
```

returns mesh-point values of $M(\xi)$ in the vector $\boldsymbol{M}$. Now it remains to explain how to construct the mapping $\boldsymbol{f}$ using the SCT.

Let us consider the case of a submerged rectangular obstruction, in its symmetric configuration, namely an example where $\mathrm{d}f/\mathrm{d}w$ cannot be integrated analytically. The geometry is presented in figure 3. The data for the Schwarz–Christoffel mapping are the location of the corners in the z-plane and the values of the internal angles at these corners, usually denoted as $\alpha_j\pi$. For example, the first and second corners are at $z = -0.5$ and $z = -0.5 + 0.5\mathrm{i}$, having $\alpha_1 = 1/2$ and $\alpha_2 = 3/2$. These are the values needed in the vectors $\boldsymbol{z}$ and ***alpha*** given below. The SCT convention is that ***inf*** indicates a polygon 'corner at infinity' with angle $\alpha = 0$. Also, there are two points which help define the reflected upper boundary of the symmetric domain, namely the

https://doi.org/10.1017/jfm.2012.19 Published online by Cambridge University Press

points at $z = 4 + 2\mathrm{i}$ and $z = -4 + 2\mathrm{i}$. There are no corners at these points, so the angle for both is π, which leads to $\alpha = 1$. In summary, the input data and commands for constructing the mapping function $f(w)$ are

```
>> z=[-inf, -0.5, -0.5+0.5*i, 0.5+0.5*i, 0.5, inf, 4+2i, 0.5+2*i,...
      0.5+1.5*i, -0.5+1.5*i, -0.5+2*i, -4+2i];
>> alpha=[0., .5, 1.5, 1.5, 0.5, 0., 1., .5, 1.5, 1.5, 0.5, 1. ];
>> p=polygon(z,alpha);
>> f=stripmap(p)
```

The command ***polygon*** defines, within the SCT framework, a polygonal object to be conformally mapped onto a strip through the command ***stripmap***. A window will open asking the user to confirm the points at infinity, as indicated in red on the screen. Clicking on the left 'infinity-node' first and then on the 'right-infinity' node, immediately the SCT executes the mapping and prints on the screen the values of the relevant parameters, including each vertex's pre-image, referred to as a *prevertex*:

```
f =

  SC stripmap:

     vertex                alpha           prevertex
 ------------------------------------------------------------
     -Inf + 0.00000i       0.00000                    -Inf
 -0.50000 - 1.00000i       0.50000      0.000000000000e+00
 -0.50000 - 0.50000i       1.50000      2.206649804916e-01
  0.50000 - 0.50000i       1.50000      1.387112328201e+00
  0.50000 - 1.00000i       0.50000      1.607777308619e+00
      Inf + 0.00000i       0.00000                     Inf
  4.00000 + 1.00000i       1.00000      3.178793344627e+00 + i
  0.50000 + 1.00000i       0.50000      1.607777308015e+00 + i
  0.50000 + 0.50000i       1.50000      1.387112327604e+00 + i
 -0.50000 + 0.50000i       1.50000      2.206649800609e-01 + i
 -0.50000 + 1.00000i       0.50000     -3.041898677392e-10 + i
 -4.00000 + 1.00000i       1.00000     -1.571016036835e+00 + i

  c = 2 + 1.2246468e-16i
  Apparent accuracy is 1.35e-09
```

Figure 3 is created through the command `>>plot(f,30,20)`. For more complex topographies, the only difference regarding the vectors $\boldsymbol{z}$ and ***alpha*** is that their input might be by hand (in the command line as above) or automatically generated by another code. In other words, all the SCT commands described above remain the same, including the calculation of $M(\xi)$.

Finally, we discuss the computation of the discrete values of the Jacobian along the free surface. Consider a curve described in the w-plane by its grid-point values ($w_j = \xi_j + \mathrm{i}\zeta_j$ stored in the vector $\boldsymbol{w}$). Computing the Jacobian along this curve reduces to

```
>> J = abs(evaldiff(f,w)).^2;
```

A.2. *Mapping wave profiles*

As a first example, consider the Boussinesq equations (3.35)–(3.36), with the variable coefficient $M(\xi)$ computed as above. Let the initial wave profile be $\eta(x, 0) = \eta_o(x)$. In most reflection–transmission problems, as those studied in Muñoz & Nachbin (2005, 2006), the initial wave profile is propagating from a region of constant depth towards the topography. In these cases no preprocessing of the initial profile is needed (i.e. $N_o \equiv \eta_o$) because away from the variable bottom very quickly the Jacobian approaches 1. This was indicated in figure 1. But, in general, this will not be the case and the initial wave profile $N_o \equiv N(\xi, 0)$ has to be computed from η_o. Inversion of the mapping $x + \mathrm{i}\eta(x, t) = f(\xi + \mathrm{i}N(\xi, t))$, denoted here for the initial data as

$$\xi + \mathrm{i}N_o(\xi) = f^{-1}(x + \mathrm{i}\eta_o(x)), \tag{A 3}$$

https://doi.org/10.1017/jfm.2012.19 Published online by Cambridge University Press

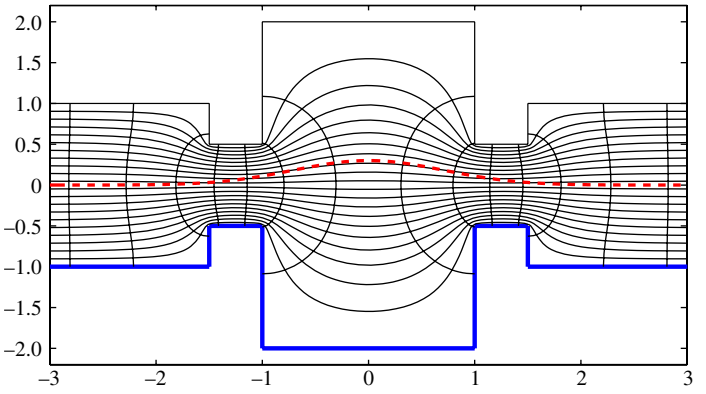


FIGURE 4. (Colour online) Symmetric channel with two submerged walls and a wide trench. The
wave profile is indicated in the dashed line. The region below the wave profile is occupied by fluid.

is obtained through the command

```
>> N = imag(evalinv(f,Z));
```

where `Z` is a vector containing the free-surface values $x_j + \mathrm{i}\eta_o(x_j)$. The imaginary part of the inverse mapping is the wave elevation in the w-plane. Moreover, at any time $t = t_n$ the wave profile $\eta(x_j, t_n)$ is recovered in the z-plane through the command

```
>> eta = imag(eval(f,W));
```

`W` is a vector containing the free-surface values $\xi_j + \mathrm{i}N(\xi_j, t_n)$ in the w-plane.

The pre- and postprocessing of the wave profile, as described above, both require using MATLAB. In the weakly nonlinear case, one can use (3.22) to expedite the mapping of wave profiles without having to access MATLAB again.

Suppose we have already evaluated $M(\xi)$ at the mesh points ξ_j (stored in the vector `xi`) and that we have also established the free-surface mesh-point correspondence $\xi_j \to x_j$. This is obtained through `>>x = real(evalinv(f,xi+0.5*i));`

We are now in position to solve the Boussinesq system for different initial data without pre- or postprocessing the wave profiles within MATLAB. We simply use the approximation given in (3.22):

$$N(\xi_j, t) \approx \frac{\eta(x_j, t)}{M(\xi_j)}. \tag{A 4}$$

This *approximate* wave-profile mapping can be used at any time t. In figure 5, we illustrate the quality of this approximation in the presence of a very abrupt bottom variation as shown in figure 4. For waves of moderate amplitude, the approximation is quite effective.

Appendix B. Linear dispersion analysis

In this section, we perform a linear dispersion analysis along the lines of AFM, § 3. For simplicity, consider the 2D equations (2.14)–(2.16) in the linear ($\varepsilon = 0$) regime. Namely, let

$$q_t + \eta = 0, \tag{B 1}$$

https://doi.org/10.1017/jfm.2012.19 Published online by Cambridge University Press

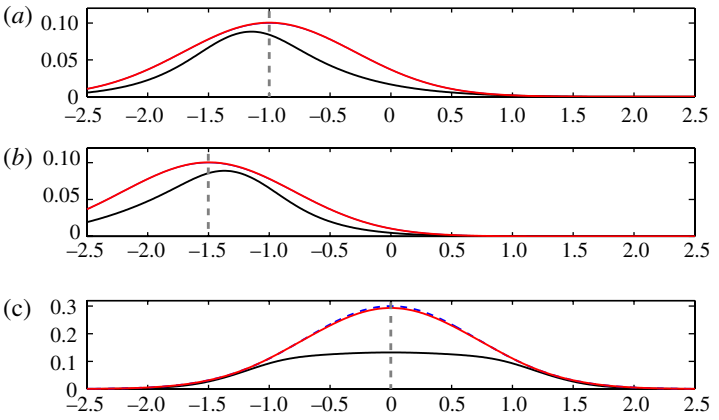


FIGURE 5. (Colour online) Symmetric channel with two submerged walls and a wide deep trench. The wave profiles presented are Gaussians centred at the points indicated by the dashed lines. In the two top figures the wave amplitude is equal to 0.1 and the profiles are centred above each corner of the left submerged wall. In the bottom figure a Gaussian wave profile of larger amplitude (equal to 0.3) is centred at the origin. In each figure the top solid curve is η equal to the corresponding Gaussian; the bottom solid curve is $N = \mathrm{Im}\{f^{-1}(x+\mathrm{i}\eta)\}$, the wave profile in the w-plane; the top dashed line (only visible in the bottom figure) is the approximation (A 4), indicating its accuracy.

$$\int_{-\infty}^{\infty} \mathrm{d}x\, \mathrm{e}^{\mathrm{i}kx} \left\{ \mathrm{i}\eta_t \cosh[k\mu] + \frac{q_x}{\mu} \sinh[k\mu] + \frac{\Phi_x}{\mu} \sinh[k\mu H] \right\} = 0, \quad k \in \mathbb{R}, \tag{B 2}$$

$$\int_{-\infty}^{\infty} \mathrm{d}x\, \mathrm{e}^{\mathrm{i}kx} \left\{ \mathrm{i}\eta_t \sinh[k\mu] + \frac{q_x}{\mu} \cosh[k\mu] - \frac{\Phi_x}{\mu} \cosh[k\mu H] \right\} = 0, \quad k \in \mathbb{R}. \tag{B 3}$$

Define $\varphi(x; k, \mu) \equiv \Phi_x \cosh[k\mu H]$ and use (B 1) so that the non-local relations are written as

$$\int_{-\infty}^{\infty} \mathrm{d}x\, \mathrm{e}^{\mathrm{i}kx} \left\{ -\mathrm{i}q_{tt} \cosh[k\mu] + \frac{q_x}{\mu} \sinh[k\mu] + \frac{\varphi}{\mu} \tanh[k\mu H] \right\} = 0, \quad k \in \mathbb{R}, \tag{B 4}$$

$$\int_{-\infty}^{\infty} \mathrm{d}x\, \mathrm{e}^{\mathrm{i}kx} \left\{ -\mathrm{i}q_{tt} \sinh[k\mu] + \frac{q_x}{\mu} \cosh[k\mu] - \frac{\varphi}{\mu} \right\} = 0, \quad k \in \mathbb{R}. \tag{B 5}$$

Equation (B 5) yields the Fourier transform of the auxiliary function φ as

$$\frac{\hat{\varphi}}{\mu} = -\mathrm{i}\hat{q}_{tt} \sinh[k\mu] - \mathrm{i}k \frac{\hat{q}}{\mu} \cosh[k\mu], \quad k \in \mathbb{R}. \tag{B 6}$$

Performing a frozen coefficient analysis, we set $\tanh[k\mu H_j]$ to be a generic (frozen) value at some point $x = x_j$. Substitution of (B 6) in (B 4) yields the evolution equation

$$\hat{q}_{tt} + \tilde{\omega}^2 \hat{q} = 0, \tag{B 7}$$

where

$$\tilde{\omega}^2 \equiv \frac{\omega^2 + (k/\mu)\tanh(k\mu H_j)}{1 + (\mu/k)\tanh(k\mu H_j)}. \tag{B 8}$$

Recall that $\omega^2 \equiv (k/\mu)\tanh(k\mu)$.

https://doi.org/10.1017/jfm.2012.19 Published online by Cambridge University Press

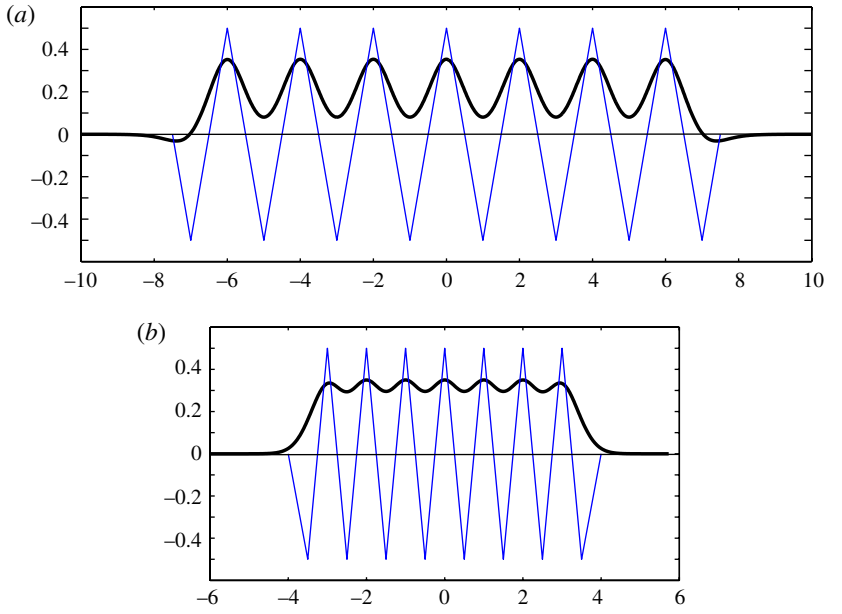


FIGURE 6. (Colour online) A mean-zero (sawtooth-like) topography profile $-H(x)$ of period equal to 2 (*a*) and equal to 1 (*b*), both of height equal to 0.5 (half the depth). The smooth curve represents the variable coefficient $m(\xi(x))$.

Repeating this linear analysis with (3.23)–(3.24), by setting $\varepsilon = 0$, we get

$$\int_{-\infty}^{\infty} \mathrm{d}\xi \mathrm{e}^{\mathrm{i}k\xi} \left\{ \mathrm{i}|\mathrm{J}|N_t \cosh[k\mu] + \frac{q_\xi}{\mu} \sinh[k\mu] \right\} = 0, \quad k \in \mathbb{R} \tag{B 9}$$

and

$$q_t + \eta = 0. \tag{B 10}$$

In the linear case, $|\mathrm{J}| = M^2(\xi)$ and $N = \eta/M$. Therefore,

$$\int_{-\infty}^{\infty} \mathrm{d}\xi \mathrm{e}^{\mathrm{i}k\xi} \left\{ -\mathrm{i}M(\xi) q_{tt} \cosh[k\mu] + \frac{q_\xi}{\mu} \sinh[k\mu] \right\} = 0, \quad k \in \mathbb{R}, \tag{B 11}$$

and by a frozen coefficient analysis

$$\hat{q}_{tt} + \tilde{\omega}^2 \hat{q} = 0 \quad \text{with } \tilde{\omega}^2 \equiv \omega^2/M_j. \tag{B 12}$$

The frequencies $\tilde{\omega}$ are different whether the linear non-local formulation is in Cartesian coordinates (x, y) or in curvilinear coordinates (ξ, ζ). In particular, consider the case where $|H| < 1$ together with the long-wave regime, so that

$$\frac{k}{\mu} \tanh(k\mu H_j) = k^2 H_j - \frac{\mu^2 k^4 H_j^3}{3} + \cdots, \tag{B 13}$$

$$\frac{\mu}{k} \tanh(k\mu H_j) = \mu^2 H_j - \frac{\mu^4 k^2 H_j^3}{3} + \cdots. \tag{B 14}$$

To leading order, the tanh term in the numerator of (B 8) has derivatives of H. In the case of rapidly varying bottom variations, denoted by $H(x/\delta)$ ($\delta \ll 1$), the range of the

https://doi.org/10.1017/jfm.2012.19 Published online by Cambridge University Press

frequency $\tilde{\omega}$ will be enlarged by factors of the order of $1/\delta^2$, as a manifestation of the high-frequency forcing by the topography. In the conformal mapping framework this does not happen. Actually, the formulation automatically performs an averaging of the high-frequency forcing, as will be shown below.

Recall from (2.7) that $H' = h_o(1 + H)$, so that the dimensionless topography profile is denoted by $-H(x)$. Having this in mind, write $M(\xi)$ as

$$y_\xi(\xi, \zeta_o) = M(\xi) \equiv 1 - m(\xi), \tag{B 15}$$

which allows an interpretation of $m(\xi)$ as the topographic forcing expressed at the undisturbed free-surface level ζ_o. By employing the SCT, the values of $m(\xi)$ are readily available for display and for comparison with the bottom profile. At the top of figure 6, a sawtooth topography of period 2 is displayed together with a thicker line representing $m(\xi)$. In the bottom part of figure 6, the period of the sawtooth topography is reduced to 1 and an averaging effect is observed in the profile of m. In other words, the sharp, highly fluctuating topography is felt along the free surface as a smooth (elevation) bump with small-amplitude corrugations. Namely, in this regime the free-surface dynamics will not detect the deep sharp valleys of the topography. In Nachbin (2003), $M(\xi)$ was written as a convolution of a smooth kernel with $1 + H(x)$, which also reflects the averaging described above.

REFERENCES

Ablowitz, M. J., Fokas, A. S. & Musslimani, Z. H. 2006 On a new non-local formulation of water waves. *J. Fluid Mech.* **562**, 313–343.

Artiles, W. & Nachbin, A. 2004 Nonlinear evolution of surface gravity waves over highly variable depth. *Phys. Rev. Lett.* **93**, 234501-1.

Ashton, A. C. L. & Fokas, A. S. 2011 A non-local formulation of rotational water waves. *J. Fluid Mech.* **689**, 129–148.

Deconinck, D. & Oliveras, K. 2011 The instability of periodic surface gravity waves. *J. Fluid Mech.* **675**, 141–167.

Driscoll, T. A. & Trefethen, L. 2002 *Schwarz–Christoffel Mapping*. Cambridge University Press.

Floryan, J. M. 1985 Conformal-mapping based coordinate generation method for channel flows. *J. Comput. Phys.* **58**, 229–245.

Fokas, A. S. 2000 On the integrability of linear and nonlinear partial differential equations. *J. Math. Phys.* **41** (6), 4188–4237.

Fokas, A. S. & Sung, L. Y. 2005 Generalised Fourier transforms, their nonlinearization and the imaging of the brain. *Not. AMS* **52**, 1176–1190.

Garnier, J., Kraenkel, R. A. & Nachbin, A. 2007 Optimal Boussinesq model for shallow-water waves interacting with a microstructure. *Phys. Rev.* E **76**, 046311.

Haut, T. S. & Ablowitz, M. J. 2009 A reformulation and applications of interfacial fluids with a free surface. *J. Fluid Mech.* **631**, 375–396.

Keller, J. 2003 Shallow-water theory for arbitrary slopes of the bottom. *J. Fluid Mech.* **489**, 345–348.

Mei, C. C., Stiassnie, M. & Yue, D. K.-P. 2005 *Theory and Applications of Ocean Surface Waves, Part 2: Nonlinear Aspects*. World Scientific.

Muñoz, J. C. & Nachbin, A. 2005 Stiff microscale forcing and solitary wave refocusing. *SIAM Multiscale Model. Simul.* **3** (3), 680–705.

Muñoz, J. C. & Nachbin, A. 2006 Improved Boussinesq-type equations for highly-variable depths. *IMA J. Appl. Maths* **71**, 600–633.

Nachbin, A. 2003 A terrain-following Boussinesq system. *SIAM J. Appl. Maths* **63** (3), 905–922.

Nwogu, O. 1993 Alternative form of Boussinesq equations for nearshore wave propagation. *J. Waterway Port Coast. Ocean Engng* **119** (6), 618–638.

https://doi.org/10.1017/jfm.2012.19 Published online by Cambridge University Press

PEREGRINE, D. H. 1967 Long waves on a beach. *J. Fluid Mech.* **27**, 815–827.

RUIZ DE ZÁRATE, A. R., ALFARO-VIGO, D. G., NACHBIN, A. & CHOI, W. 2009 A higher-order internal wave model accounting for large bathymetric variations. *Stud. Appl. Maths* **122**, 275–294.

XU, L. & GUYENNE, P. 2009 Numerical simulation of three-dimensional nonlinear water waves. *J. Comput. Phys.* **228**, 8446–8466.

https://doi.org/10.1017/jfm.2012.19 Published online by Cambridge University Press